J Mater Sci: Mater Electron (2016) 27:2534–2544
DOI 10.1007/s10854-015-4056-2

A novel double-incidence and multi-band left-handed metamaterials composed of double Z-shaped structure

Houqian Zhou[1] · Chunhua Wang[1] · Hao Peng[1]

Received: 2 August 2015 / Accepted: 8 November 2015 / Published online: 14 November 2015

Abstract In this paper, a novel double-incidence and multi-band left-handed metamaterial (LHM) was presented based on coplanar electric and magnetic resonators, whose structure is composed of two orthogonal Z-shaped metallic strips on each side of the dielectric substrate respectively. Both the double Z-shaped LHM for electromagnetic wave parallel and normal incidences are discussed. The structure exhibits two LH pass-bands and one right-handed pass-band when electromagnetic waves are incident parallel to the substrate, while it can achieve multiple LH pass-bands under normal incidence with the same structure and only single size of Z-shaped strips. By means of theoretical analysis, building equivalent magnetic resonance circuit models, numerical simulation, extracting the effective permittivity, permeability from S parameters and the experimental measurement, the left-handed properties are analyzed and verified. The fabricated double Z-shaped metamaterials will create a new way to prepare the electromagnetic cloak which is suitable for multiple frequencies, and the cloak of infrared or visible frequency, especially with the same structure and in same size from different incident directions.

✉ Chunhua Wang
wch1227164@hnu.edu.cn

[1] College of Computer Science and Electronic Engineering, Hunan University, Changsha 410082, People's Republic of China

1 Introduction

Left-handed metamaterials (LHMs) are artificial metamaterials with negative permittivity (ε) and negative permeability (μ) simultaneously [1, 2], which have drawn considerable attention recently in the scientific community for a series of fantastic characteristics, and for wide applications at optics such as perfect lens [3] and electromagnetic cloak [4, 5]. The first LHMs, combined with periodic arrays of split-ring-resonators (SRRs) and thin metallic wires, are experimentally demonstrated by Shelby et al. [2]. Since then many investigations have been trying to extend the negative index of refraction metamaterials to dual-band [6, 7] or multi-band [8, 9], as well as optical wavelength [10, 11].

Nowadays, the realization of dual-band, multi-band LHMs remain to be the main topic of LHM research. A great variety of LHMs have been designed and fabricated, especially Chen et al. [12] demonstrated the phenomenon of negative refraction to show that it is not produced by periodicity, and metamaterials could be realized with composite materials or fabricated with various techniques by using versatile hosting materials, which widens the scope of realizing LHMs. Generally speaking, according to the incident direction of electromagnetic waves, the existing LHMs fall roughly into three categories. The LHMs in the first category are based on the traditional incident electromagnetic waves parallel to the substrate, such as S-shaped structure [13], omega-shaped structure [14], H-shaped structure [15], compound resonator unit cells [16], nonlinear LHM [7] and single-sided LHMs [9]. LHMs in the second category, based on the incident electromagnetic wave are perpendicular to the substrate. LHMs composed of fishnet structure [17, 18], short wire-pair structures [19], double bowknot-shaped structure [20], leaf-

shaped structure [21], as well as the so-called all-dielectric LHMs [22] fall into this category. The third is that negative permittivity and negative permeability can be achieved simultaneously, not only under parallel incidence but also under normal incidence. However, only a few researchers are focusing on this route to realize the LHMs, and so far, there has been little research to achieve it. Zhu et al. [23, 24] who present multi-bands LHMs based on multiple dendritic structures cells, show that multi-bands of negative refractive indexes can be gained for parallel and normal incidences. Nevertheless, the dendritic metamaterials are composed of different size of cell pairs. According to the implementation of LHMs band, usually they can be divided into single-band, dual-band and multi-band of LHMs. The realization of single-band LHMs is common and easy, such as omega-shaped structure [14], H-shaped structure [15], short wire-pair structures [19], leaf shaped structure [21]. The common characteristic of these metamaterials is that there is only one LH pass band. In contrast, it is difficult to fabricate multi-band LHMs. By changing the geometric size of S-shaped resonator, Chen et al. [25] proposed a LHM with two LH pass bands. Wang et al. [26] have realized multiband negative refractive index by alternatively stacking arrays of left-handed units with different geometrical dimensions. Yao et al. [27] presented a multilevel dendritic structure, with simultaneously negative permeability and permittivity for electromagnetic wave parallel incidence. Later, they [28] presented the left-handed condition of the three-level dendritic structures for normal incidence. Sikder Sunbeam Islam et al. [29] designed a split-H-shaped metamaterial for multi-band frequency range under parallel incidence of electromagnetic wave. Yuan et al. [6] fabricated a dual-band planar metamaterial with two distinct electric resonances in the terahertz regime. Song et al. [11] further developed the multi-band optical LHMs based on random dendritic cells. Recently, Liu et al. [7] have demonstrated a type of nonlinear meta-atom creating a dual-band nonlinear LHM. The LHMs mentioned above are studied by different methods or from different incidence to achieve dual-band or multiband, but so far, multiband LHMs have never been achieved from parallel incidence as well as normal incidence with the same structure and in same size. Today, with the continuous development of the LHMs, to obtain multi-band and multi-directional incidence LHMs will better meet the needs of practical application.

In this paper, we introduce a novel double-incidence and multi-band LHMs based on coplanar magnetic and electric resonators. The structure is composed of two orthogonal Z-shaped metallic strips on each side of the dielectric substrate respectively. For unit cell of the proposed LHMs, the electric resonator and magnetic resonator are fabricated simultaneously on every side of the substrate with the electric resonator in the central part of the magnetic resonator, and such unit cell is very compact and space-saving. Therefore, the double Z-shaped structure is composed of multiple electric and magnetic resonators. By adjusting the dimensions of either the magnetic resonator or the electric resonator, their negative parameter frequency bands can be tuned to overlap each other, and then it exhibits multiband LH property. Based on this method, the proposed LHMs can exhibit dual negative refraction pass-bands when the electromagnetic waves are parallel incident, while it can produce multiple negative refraction pass-bands under normal incidence. The LH properties of the proposed structure are verified by subsequent numerical simulation and experiment. The method proposed in this paper could be an important guidance for LHMs' design, especially for the multiband LHMs from parallel incidence as well as normal incidence with the same structure and in same size.

2 Design of LHMs structure and theoretic analysis

Generally speaking, there is one particular negative permeability for one particular magnetic resonance. Thus, N different magnetic resonators can realize N different negative permeability. If we combine N different magnetic resonators in such a way that the size of the combined unit cell is far less than the wavelength, it is expected that the combined structure will exhibit multiple negative permeability. Compared with the selection of magnetic resonators, this kind of the electric resonators is quite convenient. Every electric resonator with proper dimensions can be used as the electric resonator to produce dipolar electric resonance and negative permittivity. Therefore, multi-band LHMs can be realized by alternatively stacking arrays of different magnetic resonators and electric resonators. Based on the above theoretical analysis, double Z-shaped LHM was designed and fabricated.

Figure 1 shows the unit cell of the LHMs we designed. Note that the bottom layer is the same as the top one except for a rotation of 90° around the z axis, and the proposed LHMs structure is referred as "double Z-shaped structure" based on its visual resemblance. Every side of the double Z-shaped structure LHMs composed of an electric resonator and a magnetic resonator as shown in Fig. 1a. Figure 1b is the Top layer where the black parts denote metallic strips while the white parts denote the substrate. Figure 1c is the bottom layer, its geometrical dimension is the same as the top layer completely. Figure 1b shows that the square metallic ring with two splits serves as a magnetic resonator, while the oblique copper arm in the center blank part of the square ring acts as an electric resonator. In addition, in order to lower and tune the resonant frequency

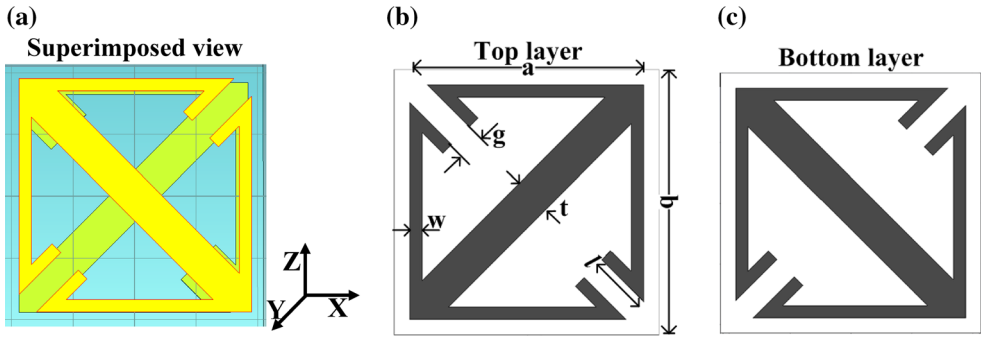

Fig. 1 **a** Superimposed view of a unit cell of the proposed LHM. **b** The *top layer* of the pattern. The *white* region corresponds to the dielectric substrate, and the substrate is FR4 (dielectric constant ε = 4.3, thickness d = 2.4 mm). The metallic pattern (*black color*) consists of the Z-shapes strips. The dimensions are: a = 7.5, b = 8.5, l = 1.4, t = 1.2, g = 0.6, and w = 0.4 mm, and the metallic material we used is copper (conductivity $\sigma = 5.8 \times 10^7$ S/m, thickness h = 0.03 mm). **c** The *bottom* layer of the pattern

of LHMs, we add two short metallic wires at every opening. So, we fabricated LHM has multiple electric and magnetic resonators. The electric resonator can realize negative ε while the magnetic resonator can realize negative μ. By adjusting the geometrical dimensions of the resonators carefully, their negative response frequency ranges can be tuned to overlap, and then simultaneous negative permeability and permittivity can be realized in the overlapped frequency ranges, thus the multi-band of negative refractive indexes is obtained.

To analyze whether this two-dimensional double Z-shaped structure based on the coplanar electric and magnetic resonators could present left-handed behavior in some certain frequency ranges, we set up equivalent LC circuit models for magnetic responses under both parallel incidence and normal incidence (two kinds of incident cases, generating different magnetic resonance circuits).

2.1 Parallel incidence

For electromagnetic wave incident parallel to the plane of the double Z-shaped structure along the x axis direction ($\boldsymbol{k}\|\boldsymbol{x}$), the electrical polarization is along the y axis direction ($\boldsymbol{E}\|\boldsymbol{y}$), and the magnetic polarization is along the z axis direction ($\boldsymbol{H}\|\boldsymbol{z}$) perpendicular to the plane. Because each side of the double Z-shaped structure could be considered as the combination of electric resonator (oblique copper arms) and magnetic resonator (square metallic ring with two splits), as shown in Fig. 1a, the magnetic field H is perpendicular to the plane of the unit cell, that is to say, perpendicular to two magnetic resonators. Therefore, it is possible to realize two magnetic resonances in different frequency bands. At the same time, two orthogonal arms and the whole Z-shaped cell behaved as cut wires that provide multiple electric dipole resonances when the electric field E is parallel to the metamaterials plane. As the structure parameter is properly adjusted, the magnetic resonances and electric resonances could be well overlapped, and the multiple LH pass-hands are realized.

In LHMs, the magnetic resonant frequency f_m is just where the left-handed peak obtained, and it could be simply regarded as the left-handed resonant frequency f_l. The single square split ring could be described as a simple effective single-sided magnetic-LC circuit model, when the magnetic polarization is normal to the surface, as shown in Fig. 2a, where L1 is the effective inductance of the short metallic wire, L2 is the effective inductance of square metallic strips, L3 is the effective inductance of the oblique metallic arm connecting the strips of the magnetic resonator, C1 is the effective capacitance between the two metallic strips. The single-side magnetic resonant frequency can be obtained by $f_{m1} = 1/2\pi\sqrt{L_e C_e}$. The total inductance of the magnetic resonator can be obtained by Le = (L1 + L2) L3/(L1 + L2 + L3). L1, L2 and L3 can be approximated by:

$$L_1 \approx A\frac{\mu_0 l}{\pi}\ln\left(\frac{4l}{w}\right), \tag{1}$$

$$L_2 \approx A\frac{\mu_0 a}{\pi}\ln\left(\frac{4a}{w}\right), \tag{2}$$

$$L_3 \approx A\frac{\mu_0 c}{\pi}\ln\left(\frac{4c}{w}\right), \tag{3}$$

where l is the effective length of the short metallic wire, a is the length of the metal strip, c is the length of the oblique copper arm and A is the modifying coefficient [23]. The capacitance is:

$$C_1 \approx \frac{\varepsilon_0 \varepsilon r' s}{d} = \frac{\varepsilon_0 \varepsilon_r' lh}{g}, \tag{4}$$

$$C_e = 2C_1 \approx 2 * \varepsilon_0 \varepsilon_r' \frac{lh}{g}, \tag{5}$$

where $\varepsilon r'$ is the relative permittivity, which is the ratio of the permittivity of the substrate to that of free space and

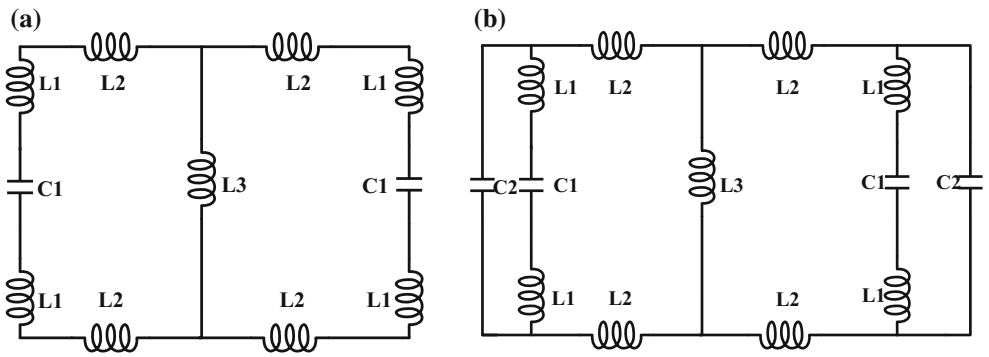

Fig. 2 The equivalent LC circuits model: **a** Single-sided magnetic resonance and **b** double-sided coupling magnetic resonance

g is the distance between the two short metallic wires. Therefore,

$$f_{m1} = \frac{1}{2\pi\sqrt{LeCe}} \sim A' \frac{tw}{al} \cdot \frac{1}{\sqrt{Ce}} \tag{6}$$

where a' is the modifying factor.

2.2 Normal incidence

For electromagnetic wave normal incidence along the z axis direction ($\boldsymbol{k}|\boldsymbol{z}$), the electrical polarization is along the y axis direction ($\boldsymbol{E}|\boldsymbol{y}$), and the magnetic polarization is along the x axis direction ($\boldsymbol{H}|\boldsymbol{x}$). In analogy to the fishnet LHMs [17, 18], metallic Z-shaped cell pairs with two different arrangements can achieve left-handed characteristic. Based on the analysis above, it can be known that the magnetic resonances are originated from the square split rings and the electric resonances are still mainly provided by the oblique copper arms. But different from parallel incidence, in addition to producing two different single-side magnetic resonances, the double Z-shaped structure could contribute to the third magnetic resonance due to the coupling between the square split-rings on both sides of the substrate when the magnetic polarization is parallel to the surface, and the third magnetic resonator could be described as the effective double-sided coupling magnetic-LC circuit model shown in Fig. 2b, where C2 is the effective capacitance between the two parallel split rings on both sides of the substrate. The additional magnetic resonance frequency can be obtained by $f_{m2} = 1/2\pi\sqrt{L_m C_m}$, where Lm = Le and Cm = 2(C1 + C2). As a result,

$$f_{m2} = \frac{1}{2\pi\sqrt{L_m C_m}} \sim B' \frac{tw}{al} \cdot \frac{1}{\sqrt{C_m}}, \tag{7}$$

where b' is the modifying factor and

$$C_2 \approx \frac{\varepsilon' s}{d} = \frac{\varepsilon' a^2}{d}, \tag{8}$$

$$C_m \approx \frac{2\varepsilon lh}{g} + \frac{2\varepsilon' a^2}{d} \tag{9}$$

Here, we indicate that these formulas for the effective inductances and capacitances are carried out on the assumption that the metal could be considered as a perfect conductive metal. Thus, it could only be used at microwave frequency or lower. For high frequency, such as terahertz and optical frequencies, the metal could not be simply considered as a perfect conductive metal, and the effective LC analysis is less accurate.

The analysis above shows that the single-sided and double-sided-coupling magnetic resonant frequencies are affected by the geometric dimensions of the magnetic resonators and the substrates. By optimized design, there will be a LHM composed of electric resonators and magnetic resonators as expected, and it can exhibit dual magnetic resonances for electromagnetic wave parallel incidence, multiple magnetic resonances for normal incidence.

3 Simulation and analysis

In order to verify the multiband LHMS, numerical simulation is first carried out by using the frequency domain solver of CST MICROWAVE STUDIO.

3.1 Parallel incidence

For electromagnetic wave parallel incidence, the incident electromagnetic wave is a planar wave polarized by a magnetic field parallel to the z axis and an electric field parallel to the y axis, propagating along the x axis. The incident condition is satisfied by applying perfect magnetic boundaries to the surfaces perpendicular to the z axis and perfect electric boundaries to the surfaces perpendicular to the y axis. With the given geometric dimensions, the S21 and S11 of scattering parameters from simulations are

shown in Fig. 3. In order to verify the existence of left-handed characteristics in pass-band, we use scattering parameters retrieval to calculate permittivity, permeability and refractive index, based on S11 and S21 obtained from the simulation [30, 31]. Figure 3a shows that there are three transmission peaks at 7.3, 8.1, and 9.4 GHz respectively, which indicates three pass-bands. From Fig. 3c and d, it can be found that in 7.1–7.4, 7.5–7.8, 8.0–8.3 and 8.4–8.7 GHz the real part of the effective permittivity is negative, while the real part of the effective permeability is negative in 7.1–7.4 and 8.0–8.3 GHz. In the frequency ranges where both the real parts of effective permittivity and permeability are negative, LH pass-bands are expected. Thus, the two LH pass-bands are 7.1–7.4 and 8.0–8.3 GHz, as shown in Fig. 3b, the refractive index has negative values in two frequency ranges. The first and second pass-bands in Fig. 3a are LH, while the third one is RH.

Note that there is a RH pass-band beside the two LH pass-bands. This is in analogy to the dual-band LHM in Ref [7] where there is a RH between two LH pass-bands. The underlying reason for the difference lies in that the mechanisms and structures of realizing LH pass-bands in the two cases are different. For the dual-band LHM in Ref [7], it adopted a type of nonlinear meta-atom to create a dual-band nonlinear LHM, while we selected is double Z-shaped strips composed of coplanar magnetic and electric resonators. For the multi-band LHM we presented in this paper, both the negative permeability and permittivity are realized by negative responses. The negative response bandwidths of magnetic and electric responses are usually not equal. As a result, outside the LH pass-bands, both the permittivity and permeability are positive. Therefore, there is usually a RH pass-band beside the two LH pass-bands.

Attempting to further analyze its magnetic resonance and the place that the charge accumulation actually occurs, we examined the current distribution and magnetic field at the magnetic resonance where the dual bands of negative refractive indexes occur. Figure 4 shows the front-view surface current distribution for this structure at the inner (facing each other) metallic surfaces of the front and back slabs. From Fig. 4a and c, we find that the surface current on the front metallic slabs are opposite to the back slabs, leading to a strong negative magnetic resonance. Meanwhile, the most surprising feature is that the currents accumulate at two special positions. One is the conjunction with two up and down adjacent metallic strips (as Fig. 4a shows at frequency of 7.3 GHz), and the other is the conjunction with the split-rings and the oblique arms (as

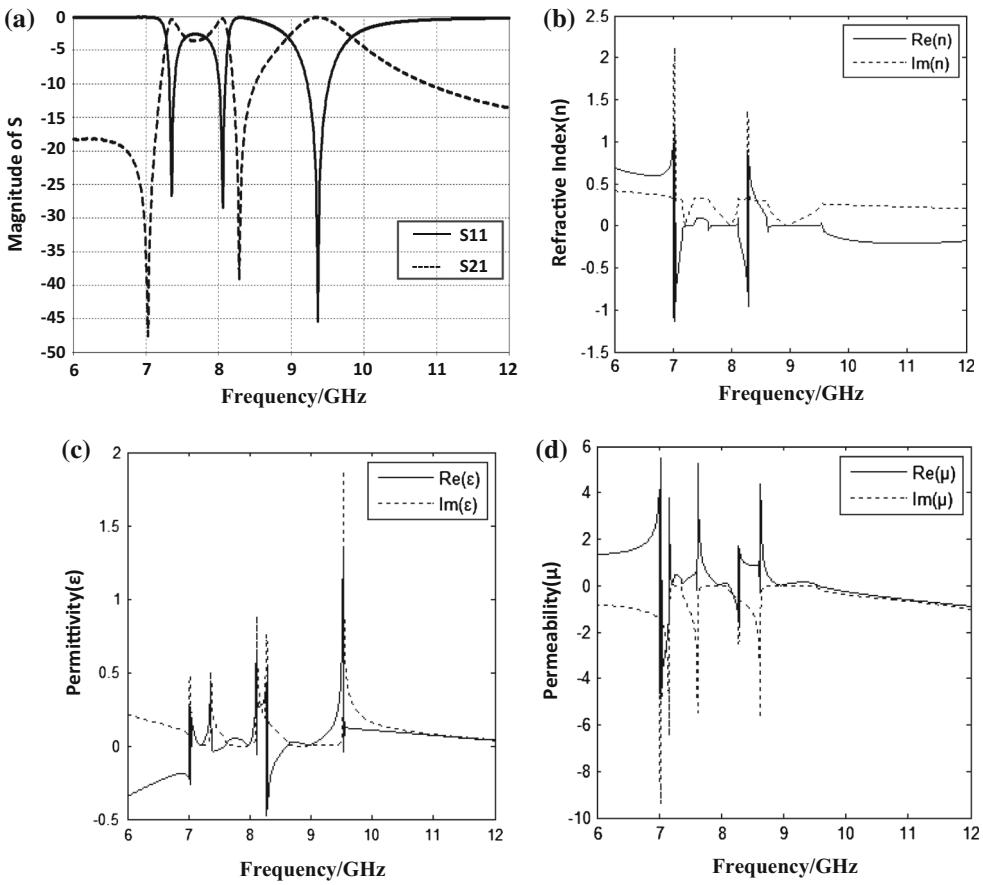

Fig. 3 The simulated transmission spectra and effective parameters of the proposed LHMs. **a** Magnitude of the simulated S parameters, **b** retrieved refractive index, **c** effective permittivity, **d** effective permeability

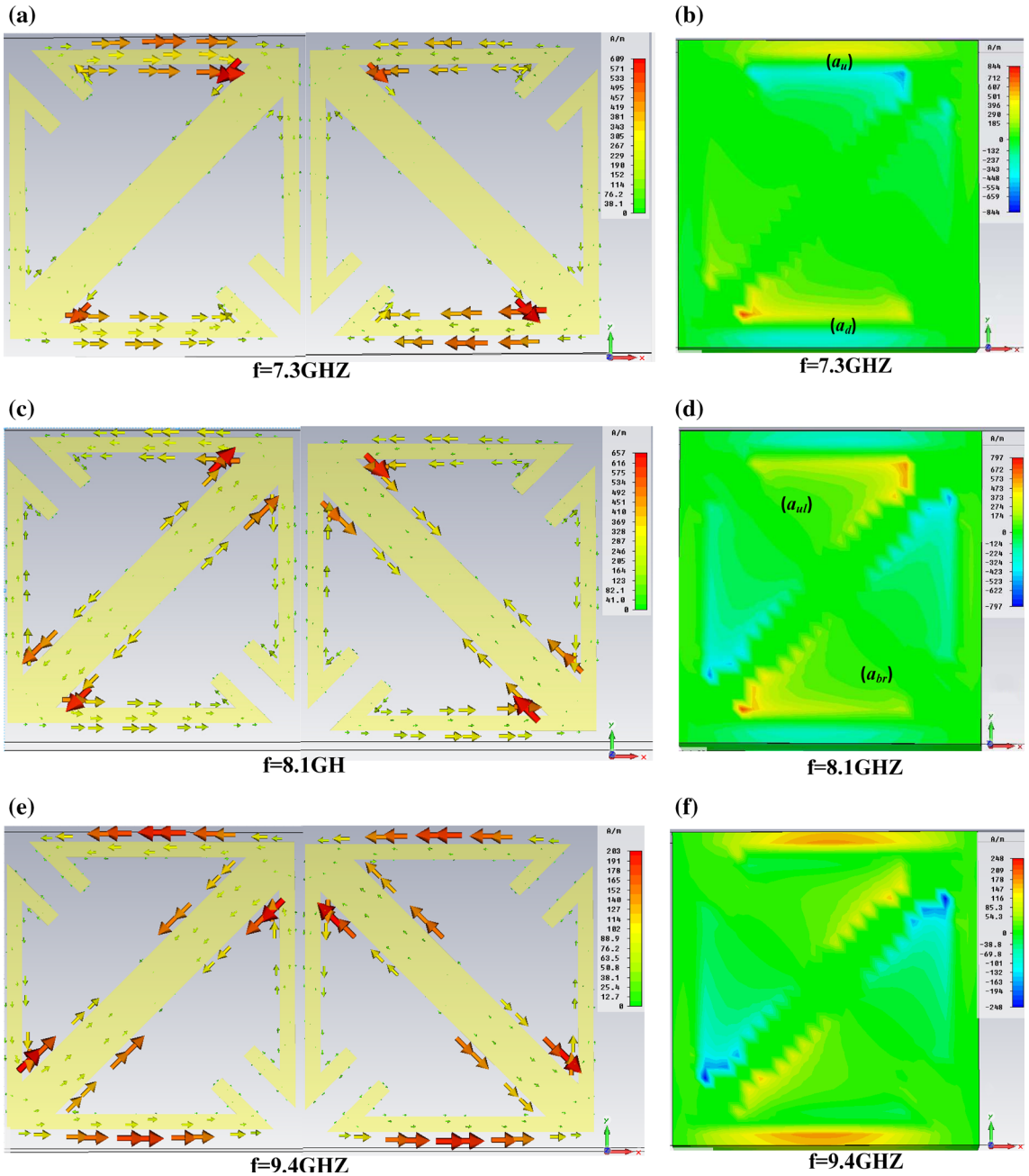

Fig. 4 Surface current distribution (*left panel*) and magnetic-field component H_z (*right panel*) for parallel incidence at frequency of 7.3, 8.1, and 9.4 GHz. (The *arrows* indicate the instantaneous current direction)

Fig. 4c shows at frequency of 8.1 GHz). Therefore, the anti-paralleled surface currents plus the displacement current in the substrate form an equivalent current loop. As we know, a current loop can be regarded as a magnetic dipole which exhibits magnetic resonance under parallel incidence of electromagnetic wave. So it is natural to explain dual negative magnetic resonances at frequency of 7.3 and 8.1 GHz. The third magnetic resonant mode (as Fig. 4e shows at frequency of 9.4 GHz) looks different from the two modes at 7.3 and 8.1 GHz. The surface current distribution on the front metallic slab is paralleled to the back slab. This resonance mode is referred as an electric polarization resonance. Many references demonstrate that the resonance frequency of the structures derives from LC circuit model, and depends on the dimensions of the structures [7, 32–34].

To validate the observed current distribution and to examine further where the charge accumulation actually

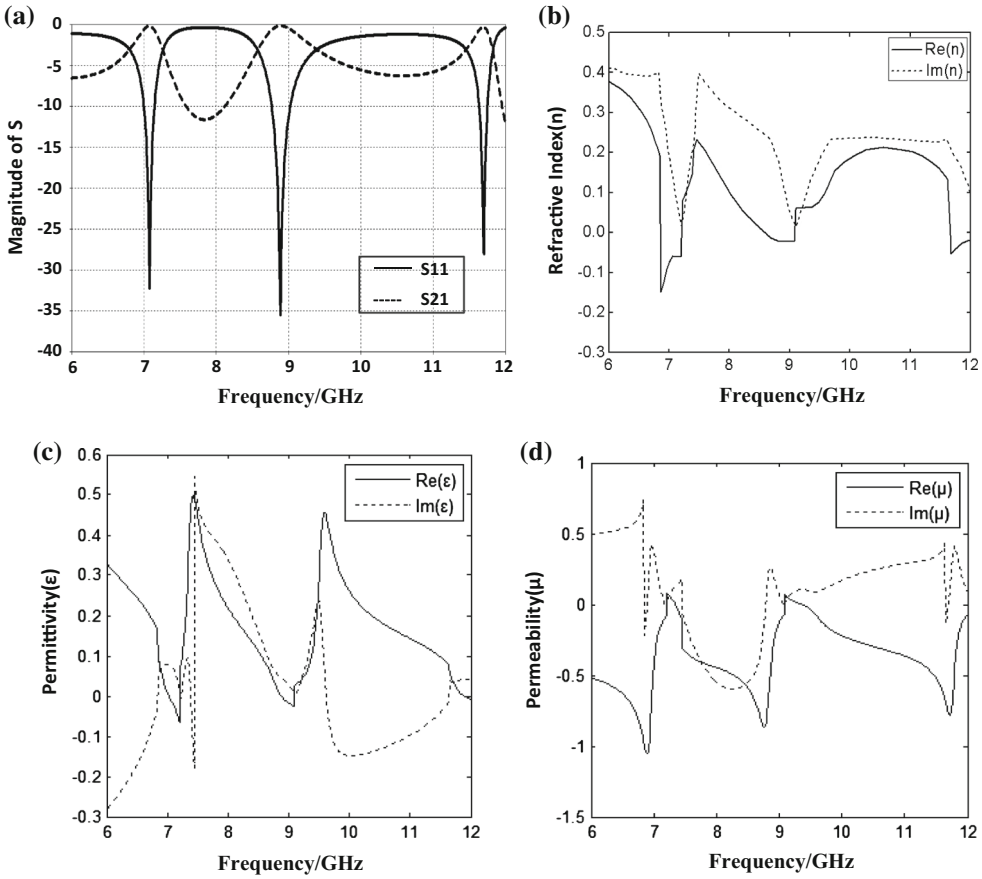

Fig. 5 The simulated transmission spectra and effective parameters of the proposed LHMs. **a** Magnitude of the simulated S parameters, **b** retrieved refractive index, **c** effective permittivity, **d** effective permeability

occurs, we examined the magnetic fields located in the middle substrate between the front and back metallic slabs. In Fig. 4, we showed the dominant magnetic field components H_z (H component in the direction of the external magnetic field). One can see that the magnetic-field intensity (as Fig. 4b, d) is consistent with the current distribution as Fig. 4a and c show. Furthermore, at $f_1 = 7.3$ GHz, magnetic field concentrates on the areas of the upside and downside in the substrate (represented as a_u and a_d, respectively), and at $f_2 = 8.1$ GHz, magnetic field produce in the areas of the upper-left and bottom-right of the substrate (represented as a_{ul} and a_{br}, respectively), which further certify that the magnetic resonances are affected by induced currents. It demonstrated that the anti-paralleled currents on the front and back metallic slabs form two equivalent loop currents in the substrate under parallel incidence, and it is just the equivalent loop currents in the substrate that produce the magnetic resonances to obtain dual negative permeability.

3.2 Normal incidence

For electromagnetic wave normal incidence, the incident condition is satisfied by applying perfect magnetic boundaries to the surfaces perpendicular to the x axis and perfect electric boundaries to the surfaces perpendicular to the y axis. In this case, the magnetic resonance is mainly produced by double metallic split-rings coupling. Although there is no change in geometrical size compared to the first model, the different boundary conditions lead to a significant variation to the resonant properties, as well as the resonant frequency. The simulated S parameters and the retrieved parameters are shown in Fig. 5. Figure 5a shows the simulated S parameters of this model. There are three transmission peaks around 7.1, 8.9 and 11.8 GHz which implies three pass-bands. From Fig. 5c and d, it can be found that in 6.8–7.3, 8.7–9.1, and 11.6–12.0 GHz, the real part of the effective permittivity is negative, while the real part of the effective permeability is negative in 6.0–7.2, 7.3–9.2 and 9.3–12 GHz. In the frequency ranges where both the real parts of effective permeability and permittivity are negative, LH pass-bands are expected. Figure 5b shows that the refractive index has negative values in three frequency ranges, and the three LH pass-bands are 6.8–7.2, 8.7–9.1 and 11.6–12 GHz. The losses in those frequency ranges are negligible, which indicates three efficient LH pass-bands.

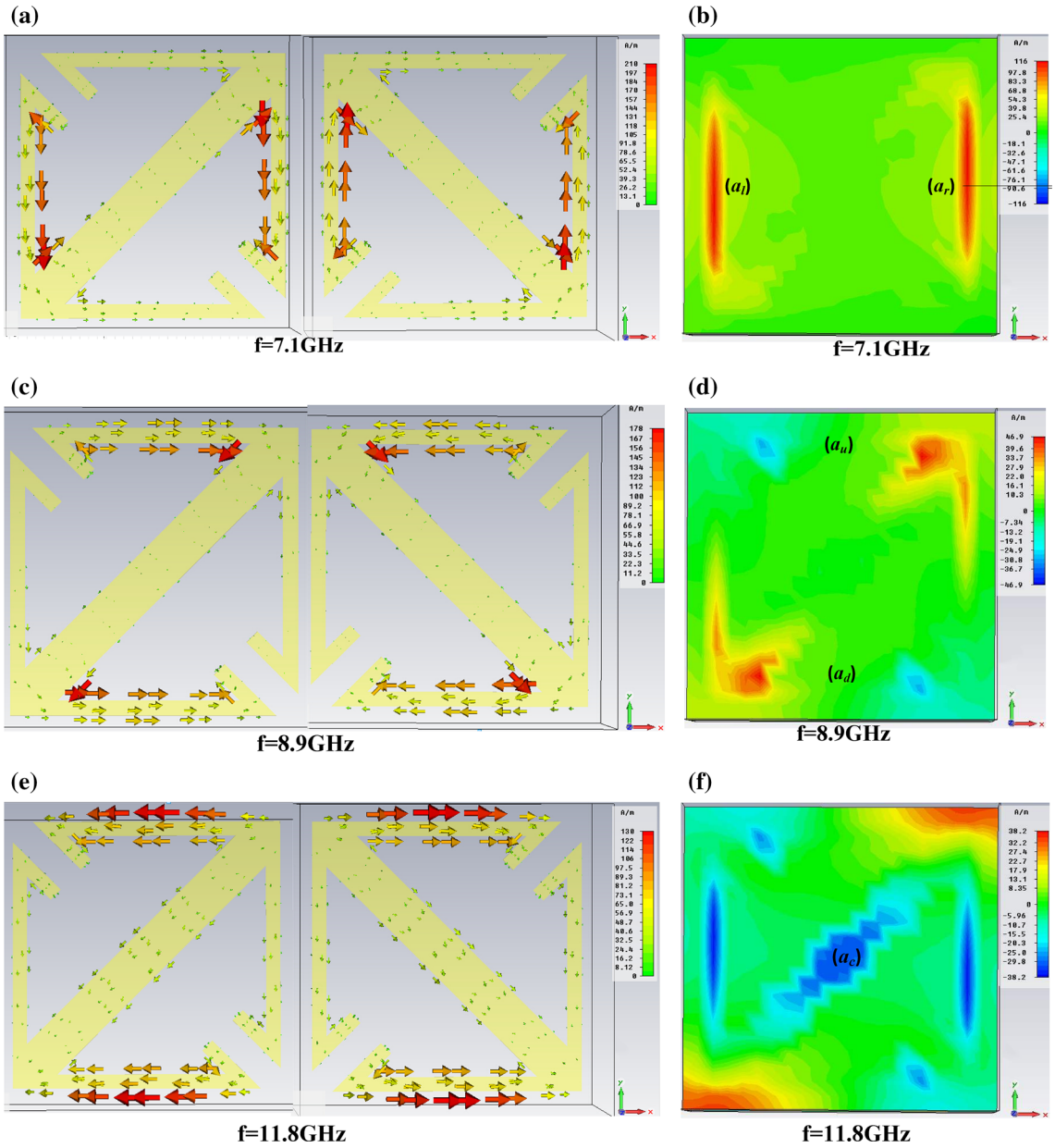

Fig. 6 Surface current distribution (*left panel*) and magnetic-field component H_x (*right panel*) for normal incidence at frequency of 7.1, 8.9, and 11.8 GHz. (The *arrows* indicate the instantaneous current direction)

To further demonstrate the resonant properties of the three peaks, surface current distributions and magnetic field are simulated as shown in Fig. 6. From Fig. 6a, c and e, we find that the orientation of the current on the front metallic slabs are anti-paralleled to the back slabs, thus producing strong charge accumulation at the areas where the two opposing flowing currents meet each other and forming three magnetic dipoles which exhibit negative magnetic resonances under normal incidence of electromagnetic wave. This feature is substantially similar to Ref [18, 21, 35]. At $f_1 = 7.1$ GHz, magnetic field concentrates on the areas of the left-side and right-side in the substrate (represented as a_l and a_r, respectively), where two loop currents are produced. So, the first left-handed band is dominated by the magnetic resonance of the areas a_l and a_r. At $f_2 = 8.9$ GHz, magnetic field produce in the areas of the upside and downside of the substrate (represented as a_u and a_d, respectively), and where two loop currents are generated. Therefore, the second left-handed band is dominated by the resonance of the areas a_u and a_d. At $f_3 = 11.8$ GHz, magnetic field is mainly localized at the center area of the "Z" pattern represented as a_c. The surface current distribution shows a loop current is produced, resulting for a magnetic resonance. Thus, the third left-handed band is

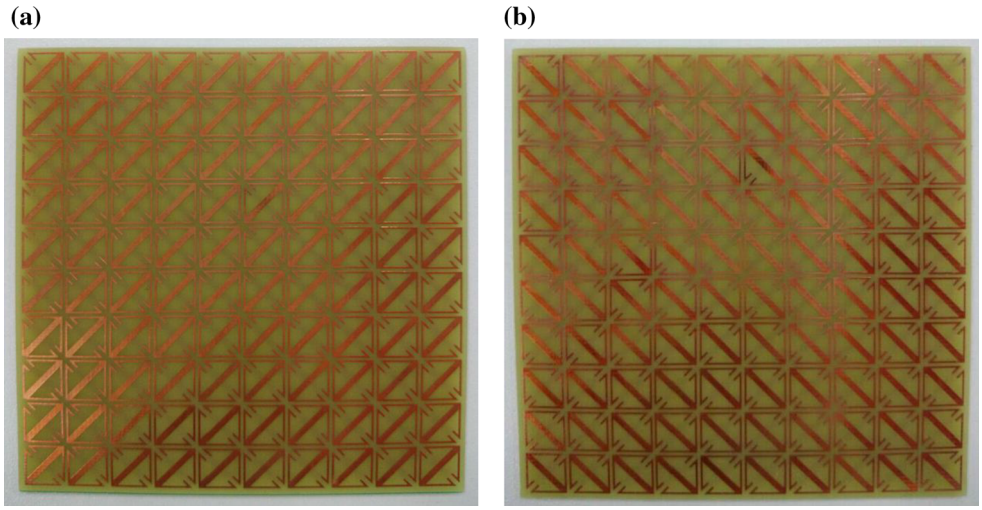

Fig. 7 Photograph of the fabricated sample: **a** *front* of the sample and **b** *back* of the sample

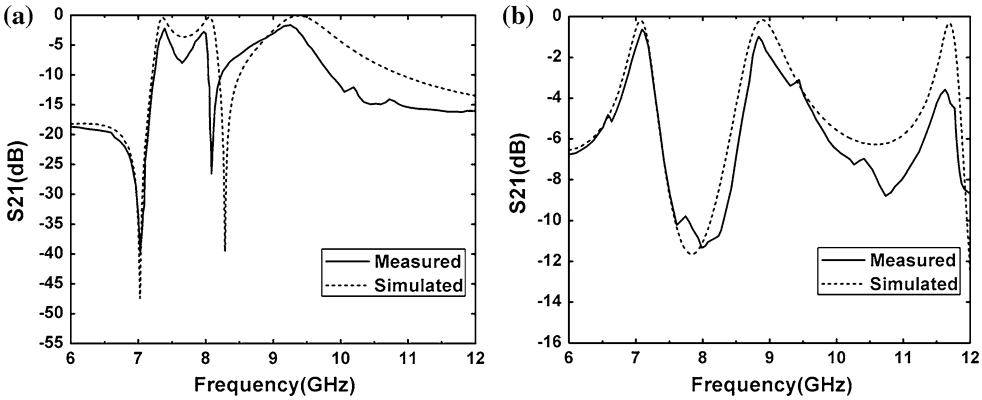

Fig. 8 Measured (*solid curve*) and simulated (*dashed curve*) transmission spectra of the proposed LHM. **a** The electromagnetic wave parallel incidence and **b** normal incidence

Table 1 Performance comparison of this work with other proposed LHMs

References	Composition or structure	Incident direction	Number of frequency bands	Frequency range	Structure complexity
[6]	Two symmetric SRRs	Normal incidence	Dual-band	Terahertz regime	Simple
[7]	Nonlinear meta-atom	Parallel incidence	Dual-band	Microwave range	Complex
[11]	Random dendritic cells	Normal incidence	Multi-band	Optical frequency	Complex
[13]	S-shaped structure	Parallel incidence	Single-band	Microwave range	Simple
[15]	H-shaped structure	Parallel incidence	Single-band	Microwave range	Simple
[19]	Short wire-pair structures	Normal incidence	Single-band	Microwave range	Simple
This work	Double Z-shaped structure	Double incidence	Multi-band	Microwave range	Simple

dominated by the resonant property of the area a_c. This is consistent with the theoretical analysis in Sect. 2. Meanwhile, from the numerical simulation, surface current and magnetic field distribution in Sect. 3, it can be confirmed that there is dual-band of negative refractive indexes for electromagnetic wave parallel incidence and multiple LH pass-bands for normal incidence. However, we are not sure which one is produced by double-sided coupling of magnetic resonance under normal incidence, which requires further research and development.

4 Experimental verification

To further verify the simulations mentioned above, we carried out the experiment verification. The experiment used for the analysis of the transmission through double Z-shaped structures includes E5071C vector network analyzer and two standard horn antennas used as an emitter and a receiver. The samples have been fabricated by using a standard printed circuit board process with 35 μm thick copper patterns on 2.4 mm thick FR4 dielectric substrate

with 10 × 10 unit cells of double Z-shaped structure in x and y directions respectively, as shown in Fig. 7. The boundary conditions along the y direction are perfect electric conditions (PEC) for electromagnetic wave either parallel or normal incidence, respectively.

The measured results of the samples are in good agreement with the simulated results as shown in Fig. 8. From Fig. 8a and b, we can find that the measured S21 parameters are almost the same as the simulated ones although there are slight shift of the resonant points. There are three transmission peaks at 7.3, 8.0, and 9.2 GHz when electromagnetic wave incidence parallel to the substrate, while those also have three pass-bands around 7.1, 8.8 and 11.6 GHz for electromagnetic wave normal incidence. Note the Fig. 8b, the first transmission peak is the highest while the third one is the lowest. This can be explained by the loss brought about by the lossy FR4 substrates. As the frequency increases, the substrate loss becomes higher, resulting in the reduction of transmission. Also note the measured transmission which is generally lower than the simulated one, and this is mainly due to the imperfection of the fabrication of the LHMs and the noise error during experiments. Eventually, in order to further discuss the advantages of the fabricated LHM, we built a table. The performance comparison of this work with other proposed LHMs is shown in Table 1, which depicts that proposed LHM has good characteristics with double incidence, multi-band, simple structure and good selectivity.

5 Conclusions

In conclusion, we proposed a double Z-shaped metamaterial based on coplanar magnetic and electric resonators can achieve multi-bands of negative refractive indexes at microwave band. The left-handed properties of the proposed structure have been verified by both numerical simulations and experiments. For electromagnetic wave parallel incidence, the structure achieves two LH pass-bands around peak of 7.3, 8.1 GHz and one RH pass-band around peak of 9.4 GHz simultaneously. For electromagnetic wave normal incidence, the structure can exhibit three LH pass-bands at the frequencies 7.1, 8.9 and 11.8 GHz simultaneously. It is the boundary conditions that make these two cases different. Furthermore, by means of setting up equivalent magnetic resonance circuit models, analyzing the surface current distribution and magnetic field of magnetic resonance, we further explained the magnetic resonance mechanism of the multiband LHM, and thus may greatly promote the development of multiband optical metamaterials. The double Z-shaped structures fabricated in this paper open a way to prepare the electromagnetic cloak suitable for multiple frequencies, and the cloak of infrared or visible frequency, especially with the same structure and in same size from different incident directions.

Acknowledgments This work is supported by the National Nature Science Foundation of China under Grant No. 61274020. The financial support is gratefully acknowledged.

References

1. V.G. Veselago, Sov. Phys. Uspekhi **10**, 509 (1968)
2. R.A. Shelby, D.R. Smith, S. Schultz, Science **292**, 77 (2001)
3. J.B. Pendry, Opt. Express **11**, 755 (2003)
4. D. Schurig, J.J. Mock, B.J. Justice, S.A. Cummer, J.B. Pendry, A.F. Starr, D.R. Smith, Science **314**, 977 (2006)
5. W. Cai, U.K. Chettiar, A.V. Kildishev, V.M. Shalaev, Nat. Photonics **1**, 224 (2007)
6. Y. Yuan, C. Bingham, T. Tyler, S. Palit, T.H. Hand, W.J. Padilla, D.R. Smith, N.M. Jokerst, S.A. Cummer, Opt. Express **16**, 9746 (2008)
7. Y.H. Liu, X. Zhou, K. Song, S. Gu, Z.J. Liu, L. Guo, X.P. Zhao, Appl. Phys. Lett. **105**, 201911 (2014)
8. G.V. Eleftheriades, I.E.E.E. Microw, Wirel. Compon. Lett. **17**, 415 (2007)
9. R.J. Gao, P.F. Shi, S.T. Liu, J. Zhao, Electron. Mater. Lett. **10**, 31 (2014)
10. Y. Yang, X.P. Zhao, H. Liu, J.K. Xiang, J. Mater. Sci.: Mater. Electron. **24**, 3330 (2013)
11. K. Song, X.P. Zhao, H.L. Ma, B.Q. Liu, J. Mater. Sci.: Mater. Electron. **24**, 4888 (2013)
12. H. Chen, L. Ran, D. Wang, J. Huangfu, Q. Jiang, J.A. Kong, Appl. Phys. Lett. **88**, 031908 (2006)
13. H.S. Chen, L.X. Ran, J.T. Huangfu, X.M. Zhang, K.S. Chen, T.M. Grzegorczyk, J.A. Kong, Phys. Rev. E **70**, 057605 (2004)
14. J.T. Huangfu, L.X. Ran, H.S. Chen, X.M. Zhang, K.S. Chen, T.M. Grzegorczyk, J.A. Kong, Appl. Phys. Lett. **84**, 1537 (2004)
15. Y.H. Liu, C.R. Luo, X.P. Zhao, Acta Phys. Sin. **56**, 5883 (2007)
16. J.F. Wang, ShB Qu, Zh Xu, J.Q. Zhang, Y.M. Yang, H. Ma, Ch. Gu, Photonics Nanostruct. Fundam. Appl. **6**, 183 (2008)
17. G. Dolling, C. Enkrich, M. Wegener, C.M. Soukoulis, S. Linden, Science **312**, 892 (2006)
18. M. Kafesaki, I. Tsiapa, N. Katsarakis, T. Koschny, C.M. Soukoulis, E.N. Economou, Phys. Rev. B **75**, 235114 (2007)
19. J. Zhou, L. Zhang, G. Tuttle, Th Koschny, C.M. Soukoulis, Phys. Rev. B **73**, 041101 (2006)
20. X. Zhou, Y.H. Liu, X.P. Zhao, Appl. Phys. A **98**, 643 (2010)
21. W.R. Zhu, X.P. Zhao, B.Y. Gong, J. Appl. Phys. **109**, 093504 (2011)
22. B. Du, J. Wang, Z. Xu, S. Xia, J.F. Wang, S.B. Qu, J. Appl. Phys. **115**, 234104 (2014)
23. W.R. Zhu, X.P. Zhao, J.Q. Guo, Appl. Phys. Lett. **92**, 241116 (2008)
24. W.R. Zhu, X.P. Zhao, J. Appl. Phys. **106**, 093511 (2009)
25. H.S. Chen, L.X. Ran, J.T. Huangfu, X.M. Zhang, K.S. Chen, T.M. Grzegorczyk, J.A. Kong, J. Appl. Phys. **96**, 5338 (2004)
26. J.F. Wang, S.B. Qu, Y.M. Yang, H. Ma, X. Wu, Z. Xu, Appl. Phys. Lett. **95**, 014105 (2009)
27. Y. Yao, X.P. Zhao, J. Appl. Phys. **101**, 124904 (2007)
28. Y. Yao, Q.H. Fu, X.P. Zhao, J. Appl. Phys. **105**, 024911 (2009)
29. S.S. Islam, M.R.I. Faruque, M.T. Islam, Appl. Phys. A **116**, 723 (2014)
30. X.D. Chen, T.M. Grzegorczyk, B. Wu, J. Pacheco Jr, J.A. Kong, Phys. Rev. E **70**, 016608 (2004)

31. D.R. Smith, D.C. Vier, Th Koschny, C.M. Soukoulis, Phys. Rev. E **71**, 036617 (2005)
32. J.B. Pendry, A.J. Holden, D.J. Robbins, W.J. Stewart, I.E.E.E. Trans, Microw. Theory Tech. **47**, 2075 (1999)
33. H. Chen, L. Ran, J. Huangfu, T.M. Grzegorczyk, J.A. Kong, J. Appl. Phys. **100**, 024915 (2006)
34. L. Ran, J. Huangfu, H. Chen, X. Zhang, K. Cheng, T.M. Grzegorczyk, J.A. Kong, Prog. Electromagn. Res. **51**, 249 (2005)
35. M.H. Li, H.L. Yang, Y. Tian, D.Y. Hou, J. Magn. Magn. Mater. **323**, 607 (2011)